Heliyon 9 (2023) e17628

Contents lists available at ScienceDirect

Heliyon

journal homepage: www.cell.com/heliyon

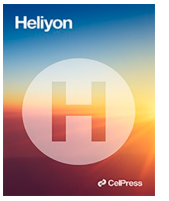

Insights into an analytical simulation of a natural convection flow controlled by Arrhenius kinetics in a micro-channel

Muhammed Murtala Hamza [a], Godwin Ojemeri [b,*], Samaila Kenga-kwai Ahmad [a]

[a] Department of Mathematics, Faculty of Physical and Computing Sciences, Usmanu Danfodiyo University, P. M. B. 2346, Sokoto State, Nigeria
[b] Department of Mathematics, College of Sciences, Federal University of Agriculture, Zuru, P. M. B. 28, Kebbi State, Nigeria

ARTICLE INFO

Keywords:
Homotopy perturbation method (HPM)
Chemically reacting fluid
Rarefaction
Magnetohydrodynamics (MHD)
Microchannel
Wall ambient temperature ratio

ABSTRACT

The focus of this paper is the investigation of an Arrhenius-driven chemical reaction in an upstanding micro-channel over an imposed transverse magnetic field with fully developed constant free convection flow. Subject to suitable boundary conditions, the temperature and velocity equations are resolved in non-dimensional form employing the homotopy perturbation method (HPM). the fundamental flow behaviors of temperature, velocity, and volumetric flow are explored as a consequence of regulating characteristics such as fluid-wall interaction parameter, rarefaction parameter, chemical reaction parameters, wall-ambient temperature difference ratio, and Hartman number. The findings are carefully investigated and graphically represented in several mesh grid graphs. It was established that increasing the values of the rarefaction parameters and chemical reaction results in an upsurge in the fluid velocity and volume flow rate, respectively, whereas increasing the Hartman number results in observable flow retardation. Additionally, when the chemical reactant parameter is ignored, the numerical comparison is in excellent agreement with the previously published results.

1. Introduction

Microfluidics and heat transfer problems have grown in prominence in the past few decades largely because of the broad spectrum of cooling-related uses they provide for manufacturing and fabrication, micro heat pipes, aerospace, micro-channel heat sink, high-performance density chips in supercomputers, and other electronic devices. Since most of these compositions are internal micro-channel flows, understanding the flow behavior becomes essentially critical for appropriate and precise projections and formulation [1,2]. New studies on the effects of fluid flow on microgeometry under different natural conditions have been published. In an up-flow microchannel with an applied magnetic field, Jha and Malgwi [3] studied the effects of Hall current and ion slip constraints on hydromagnetic free convection. Later, Jha and Aina [4] looked closely at hydromagnetic convection flow in an upright microchannel constructed from two immeasurable, electrically non-conductive plates. In their work, Jha et al. [5] examined how Hall current affected hydro magnetic free convection flow in an upward micro-channel. Other investigations in this area include [6,7,8,9,and10]], to name a few.

The significance of the electrically conducting fluid phenomena, also known as magnetohydrodynamics (MHD), has piqued the interest of engineers and scientists in recent years in numerous MHD applications, including MHD generators, biomaterials for wound treatment, sterilization of devices, and MHD accelerators. Electrically conducting fluids are already transported in a number of atomic

* Corresponding author.
E-mail address: godwinojemeri@gmail.com (G. Ojemeri).

https://doi.org/10.1016/j.heliyon.2023.e17628
Received 26 July 2022; Received in revised form 13 June 2023; Accepted 23 June 2023
Available online 4 July 2023

energy centers using (MHD) pumps in chemical energy technology. In addition to these advantages, a magnetic field can greatly speed up natural convection movement when the fluid is electrically conducting [11]. There have been numerous investigations into MHD convective flow in diverse physical contexts. With these concerns in mind, Chu et al. [12] discussed the thermal characteristics induced by the hybridization of Fe_3O_4 with MWCNT in a permeable cavity with viscous fluid and MHD. It is concluded from the study that heat transfer along walls is increased against Rayleigh and Darcy parameters, while the magnetic field effect is seen to lower the fluid velocity. The impact of hybrid nanofluids on hydromagnetic boundary wall flow for reactive fluids was demonstrated by Gul et al. [13]. Islam et al. [14] considered the numerical computation of natural convection heat transfer flow through the heating technique inside a prismatic enclosure saturated with Cu–H2O nanofluid and affected by two different heat boundary conditions. Their findings revealed that the magnetic number has a significant control on the fluid flow and temperature gradient. Saeed and Gul [15] inspected the hydromagnetic Casson nanofluid flow for heat and mass transfer along a non-stationary plate. Ibrahim et al. [16] deliberated on a two-dimensional simulation of free convection of the Al2O3–H2O nanofluids in a cavity having a heat source in its middle. As part of their findings, it was discovered that heat transfer is boosted drastically as Ra and nanoparticle volume fraction parameters rise, but a decaying effect is observed for mounting levels of magnetic field intensity. Aziz and Shams [17] studied the generation of entropy for the hydromagnetic Maxwell nanofluid flow having slip conditions, radiant heat, and variable thermal conductivity. Guriviredy et al. [18] modeled the effects of thermal generation and chemical reactions on magneto-hydrodynamics flow utilizing a semi-infinite shifting upward porous plate with a Soret factor. Gangadhar et al. [19] recently explored the influence of magnetic field and convective heating boundaries on second-grade nanofluid flow due to the Riga pattern. In another work, to analyze the two-dimensional MHD heat and mass transfer coefficient of a water-based nanofluid containing gyrotactic microorganisms toward an upright plate struck by a heat source or sink, Gangadhar et al. [20] proposed a unique spectrum relaxation approach.

Over time, interest in the composition of flow designs over chemically reactive fluids with MHD convection has increased due to their interesting and potential applications in transpiration cooling of reentry vehicles and rocket boosters, film evaporation in combustors, and cross-hatching on ablative surfaces [21]. Frank-Kamenetskii [22] is credited with being the first to offer a framework for reactive viscous fluids. The majority of lubricants employed in engineering and manufacturing procedures, including synthetic esters, hydrocarbon oils, polyglycols, and others, are reactive, as stated by Makinde [23]. With this goal in mind, the analytical study by Hamza et al. [24] on the effects of chemically reactive liquid flow in an up-flow porous annulus with mixed convection and thermal diffusion has been presented. Ojemeri et al. [25] studied the effects of slip and thermal diffusion on the free convective flow of a reactive fluid through an upward porous disk subjected to a radial magnetic field. Ahmad and Jha [26] studied the steady and time-dependent effects of fully developed natural convection and heat transfer flow of a viscous fluid in an upright porous tube. They discovered that steady-state and time-dependent heat transfer rates between tube layers increased over time. Jha et al. [27,28] presented reactive viscous flow in unsteady natural convection in an up-channel and a tube, respectively. The results show that increasing the reactant consumption parameter causes both the friction factor and the heat transfer at the channel surfaces to increase. Hamza [29] studied the steady and transient natural convection of an exothermic chemically reactive liquid in an up-flow channel in terms of the velocity slip factor and the Newtonian heating effect.

Due to their relevance in the emerging MEMS, engineering, and lubrication industries, there is a need to further investigate the effects of chemically reactive liquids (in the case of Arrhenius heating) through microchannels. This is because most of the lubricants used in engineering and industrial processes such as synthetic esters, hydrocarbon oils, polyglycols, etc. are reactive; hence the motivation for this study. Therefore, by using the homotopy perturbation approach to determine the effects of a chemical reactant parameter influenced by an applied magnetic field on steady natural convection in an upright microchannel, the current study extends

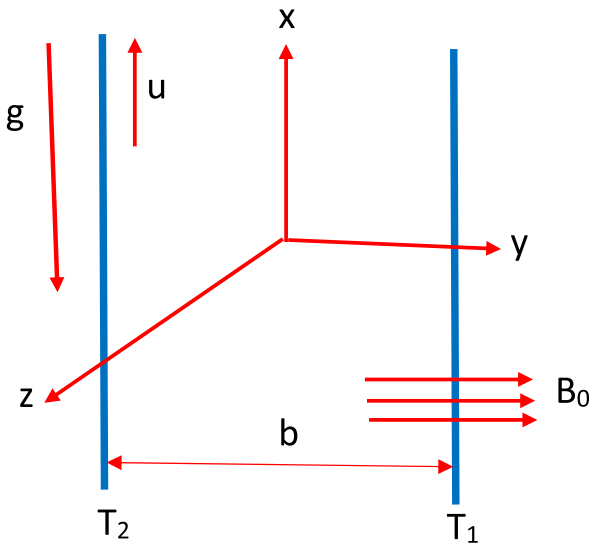

Fig. 1. The coordinate system of the flow domain.

the work of Jha et al. [2]. The unique aspect of this work is that HPM was used to provide an approximate treatment for the Arrhenius kinetics-controlled flow of viscous, electrically conductive fluid inside two upright micro-channel. The results of this study have potential applications in a variety of fields, such as biomedical engineering, microelectromechanical systems (MEMS), microdevices made using microfabrication techniques, and other therapeutic approaches. The results of this study are also crucial for establishing standards for confirming the accuracy of certain numerical or empirical methods.

2. Mathematical structure of the flow

An applied magnetic field is considered when studying the steady natural convection of a chemically reacting fluid in an upward-facing microchannel confined to two electrically non-conductive, infinitely vertical, parallel plates. The y-axis is perpendicular to the upright plate, whereas the x-axis is orthogonal to but opposite from the force of gravity, g. Fig. 1 shows the flow configuration along with the coordinate system for this flow scenario. It is proposed that a homogeneous magnetic field of B_0 strength is applied in a direction orthogonal to the flow orientation. An extremely small magnetic Reynolds number is also suspected, suggesting that the magnetic field produced would be quite small to the externally applied field. The channel surfaces are heated unevenly, with one of the plates held at T_1 while the other remains at T_2, with $T_1 > T_2$.

According to Jha et al. [2] and Hamza [29], the momentum and temperature equations for the current state are given in the basic dimensional form considering the chemically reactive parameter. This follows the fundamental idea of the Boussinesq's approximation.

$$\begin{aligned} &\upsilon\frac{d^2u'}{dy'^2}+\frac{\mu_e B_0' u'}{\rho}+g\beta(T'-T_0)=0 \quad (1)\\ &\frac{k}{\rho C_\rho}\frac{d^2T'}{dy'^2}+\frac{QC_0^*A}{\rho C_\rho}e^{\left(\frac{-E}{RT}\right)}=0 \end{aligned} \tag{2}$$

$$\left.\begin{aligned} u'(y')&=\frac{2-\sigma_v}{\sigma_v}\lambda\frac{du'}{dy'}, T'(y')=T_2+\frac{2-\sigma_v}{\sigma_v}\frac{2\gamma}{\gamma+1}\frac{\lambda}{\mathrm{Pr}}\frac{dT'}{dy'} \quad at \quad y'=0\\ u'(y')&=-\frac{2-\sigma_v}{\sigma_v}\lambda\frac{du'}{dy'}, T'(y')=T_1-\frac{2-\sigma_v}{\sigma_v}\frac{2\gamma}{\gamma+1}\frac{\lambda}{\mathrm{Pr}}\frac{dT'}{dy'} \quad at \quad y'=b \end{aligned}\right\} \tag{3}$$

Introducing the non-dimensional quantities as follows:

$$\begin{aligned} &\beta_v=\frac{2-f_v}{f_v}, \beta_t=\frac{2-f_t}{f_t}\frac{2\gamma_s}{\gamma_s+1}\frac{1}{\mathrm{Pr}}, Kn=\frac{a}{b}, In=\frac{\beta_t}{\beta_v}, \xi=\frac{T_2-T_0}{T_1-T_0}\\ &Y=\frac{y'}{b}, \theta=\frac{T-T_0}{T_1-T_0}, U=\frac{u'}{U_0}, M^2=\frac{\sigma B_0^2 b^2}{\rho v}, \mathrm{Pr}=\frac{v}{\alpha}, where \quad U_0=\frac{\rho g\beta\left(T_1'-T_0\right)b^2}{\mu}\\ &\varepsilon=\frac{RT_0}{E}, \lambda=\frac{QC_0^*AEH^2}{RT_0^2}e^{\left(\frac{-E}{RT_0}\right)} \end{aligned} \tag{4}$$

Applying equation (4) to equations (1) to (3), the dimensionless governing equations become

$$\begin{aligned} &\frac{d^2U}{dy^2}-M^2U=-\theta \quad (5)\\ &\frac{d^2\theta}{dy^2}+\lambda e^{\frac{\theta}{1+\varepsilon\theta}}=0 \end{aligned} \tag{6}$$

The relevant boundary conditions at the wall surfaces are assumed to be;

$$\left.\begin{aligned} U(Y)&=\beta_v Kn\frac{dU}{dy}, \theta(Y)=\xi+\beta_v KnIn\frac{d\theta}{dy}, at \quad y=0\\ U(Y)&=-\beta_v Kn\frac{dU}{dy}, \theta(Y)=1-\beta_v KnIn\frac{d\theta}{dy}, at \quad y=1 \end{aligned}\right\} \tag{7}$$

where M is the magnetic number, λ is the viscous heating parameter, also referred to as Frank–Kamenetskii parameter, and ε is the activation energy. It is, however, relevant to state that, in the expansion of heat source term $\lambda(1+\varepsilon\theta)^m e^{\frac{\theta}{1+\varepsilon\theta}}$, the Arrhenius heating case (i.e. when m = 0) was investigated in this article. The approximate expansion of the term $e^{\frac{\theta}{1+\varepsilon\theta}}$ is given as $e^{\frac{\theta}{1+\varepsilon\theta}} \approx 1+\theta+\ \theta^2\left(\frac{1}{2}-\varepsilon\right)+\theta^3\left(\varepsilon^2-\varepsilon+\frac{1}{6}\right)$.

3. Method of solution

3.1. Closed-form solution

To resolve the equations that govern the problem, we used the homotopy perturbation approach, creating a convex homotopy on equations (1) and (2) to obtain:

$$H(U,p) = (1-p)\frac{d^2U}{dy^2} - p\left[M^2U - \theta\right] = 0 \quad (8)$$

$$H(\theta,p) = (1-p)\frac{d^2\theta}{dy^2} + p\left[\lambda e^{\frac{\theta}{1+\varepsilon\theta}}\right] = 0 \quad (9)$$

Assume that the solutions to U and θ are in an infinite series form as:

$$\left.\begin{aligned}\theta(Y) &= \theta_0 + p\theta_1 + p^2\theta_2 + \ldots\\ U(Y) &= u_0 + pu_1 + p^2u_2 + \ldots\end{aligned}\right\} \quad (10)$$

and by inserting equation (6) into equations (4) and (5), as well as matching the coefficient of similar powers p, we obtain the sets of differential equations with the associated transformed boundary conditions:

$$p^0 : \begin{cases}\dfrac{d^2\theta_0}{dy^2} = 0\\[2ex] \dfrac{d^2u_0}{dy^2} = 0\end{cases} \quad (11)\ \&;\ (12)$$

Therefore, the transformed boundary conditions are now,

$$\left.\begin{aligned}\theta_0 &= \xi + \beta_v KnIn\frac{d\theta_0}{dy}\\ u_0 &= \beta_v Kn\frac{du_0}{dy}\end{aligned}\right\} \quad at \quad y=0 \quad (13)$$

$$\left.\begin{aligned}\theta_0 &= 1 - \beta_v KnIn\frac{d\theta_0}{dy}\\ u_0 &= -\beta_v Kn\frac{du_0}{dy}\end{aligned}\right\} \quad at \quad y=1 \quad (14)$$

$$p^1 : \begin{cases}\dfrac{d^2\theta_1}{dy^2} + \lambda\left(1 + \theta_0 + (2-\varepsilon)\theta_0^2\right) = 0\\[2ex] \dfrac{d^2u_1}{dy^2} - M^2u_0 + \theta_0 = 0\ (16)\end{cases} \quad (15)$$

Hence, the transformed boundary conditions are now,

$$\left.\begin{aligned}\theta_1 &= \beta_v KnIn\frac{d\theta_1}{dy}\\ u_1 &= \beta_v Kn\frac{du_1}{dy}\end{aligned}\right\} \quad at \quad y=0 \quad (17)$$

$$\left.\begin{aligned}\theta_1 &= -\beta_v KnIn\frac{d\theta_1}{dy}\\ u_1 &= -\beta_v Kn\frac{du_1}{dy}\end{aligned}\right\} \quad at \quad y=1 \quad (18)$$

$$p^2 : \begin{cases}\dfrac{d^2\theta_2}{dy^2} + \lambda(\theta_1 - 2\varepsilon\theta_1\theta_0 + 4\theta_1\theta_0) = 0\\[2ex] \dfrac{d^2u_2}{dy^2} - M^2u_1 + \theta_1 = 0\ (20)\end{cases} \quad (19)$$

Now, the transformed boundary conditions are given by,

$$\left.\begin{aligned}\theta_2 &= \beta_v KnIn\frac{d\theta_2}{dy}\\ u_2 &= \beta_v Kn\frac{du_2}{dy}\end{aligned}\right\} \quad at \quad y=0 \tag{21}$$

$$\left.\begin{aligned}\theta_2 &= -\beta_v KnIn\frac{d\theta_2}{dy}\\ u_2 &= -\beta_v Kn\frac{du_2}{dy}\end{aligned}\right\} \quad at \quad y=1 \tag{22}$$

Setting p to equal to1, the approximate solutions of the differential problems become:

$$\left.\begin{aligned}\theta &= \lim_{p\to 1}\theta = \theta_0+\theta_1+\theta_2+\ldots\\ U &= \lim_{p\to 1}U = u_0+u_1+u_2+\ldots\end{aligned}\right\} \tag{23}$$

Convergence for series (23) occurs for a small number of terms in most cases. However, the nonlinear operator has control over how fast the convergence occurs. According to Ayati and Biazar [30], the homotopy perturbation converges to the series solution, which highlights the fact that only a limited number of terms from the HPM results can be used to arrive at an approximate solution.

The solutions $\theta_0,\theta_1,\theta_2\ldots$ *and* $u_0,u_1,u_2\ldots$ have been derived as:

$$\theta_0 = A_0 + A_1 y \tag{24}$$

$$\theta_1 = -\lambda\left[\frac{y^2}{2}+A_0\frac{y^2}{2}+A_1\frac{y^3}{6}+(2-\varepsilon)\left(A_0^2\frac{y^2}{2}+A_0A_1\frac{y^3}{3}+A_1^2\frac{y^4}{12}\right)\right]+A_3y+A_2 \tag{25}$$

$$\begin{aligned}\theta_2 = &-(4\lambda-2\varepsilon\lambda)\left[\lambda\{A_0\frac{y^4}{24}+A_0^2\frac{y^4}{24}+A_0A_1\frac{y^5}{120}+(2-\varepsilon)\left(A_0^3\frac{y^4}{24}+A_0^2A_1\frac{y^5}{60}+A_0A_1^2\frac{y^6}{360}\right)\right\}\\ &+A_0A_3\frac{y^3}{6}+A_0A_2\frac{y^2}{2}-\lambda\left\{A_1\frac{y^5}{40}+A_0A_1\frac{y^5}{40}+A_1^2\frac{y^6}{180}+(2-\varepsilon)\left(A_0^2A_1\frac{y^5}{40}+A_0A_1^2\frac{y^6}{60}+A_1^3\frac{y^7}{504}\right)\right\}\\ &+A_3A_1\frac{y^4}{12}+A_2A_1\frac{y^3}{6}\Big]+\lambda^2\left\{\frac{y^4}{24}+A_0\frac{y^4}{24}+A_1\frac{y^5}{120}+(2-\varepsilon)\left(A_0^2\frac{y^4}{24}+A_0A_1\frac{y^5}{60}+A_1^2\frac{y^6}{360}\right)\right\}\\ &+\lambda\left(A_3\frac{y^3}{6}+A_2\frac{y^2}{2}\right)+A_5y+A_4\end{aligned} \tag{26}$$

$$u_1 = -A_0\frac{y^2}{2}-A_1\frac{y^3}{6}+D_3y+D_2 \tag{27}$$

$$u_2 = M^2\left(-A_0\frac{y^4}{24}-A_1\frac{y^5}{120}+D_3\frac{y^3}{6}+D_2\frac{y^2}{2}\right)+\lambda\left\{\frac{y^4}{24}+A_0\frac{y^4}{24}+A_1\frac{y^5}{120}+(2-\varepsilon)\left(A_0^2\frac{y^4}{24}+A_0A_1\frac{y^5}{60}+A_1^2\frac{y^6}{360}\right)\right\}-A_3\frac{y^3}{6}-A_2\frac{y^2}{2}+D_5y+D_4 \tag{28}$$

Equations 24–28 give the solutions for the energy and momentum as

$$\theta(Y) = \theta_0+\theta_1+\theta_2+\ldots$$

$$U(Y) = u_0+u_1+u_2+\ldots$$

Two crucial factors for buoyancy-driven micro heat transfers are volume flow and heat transfer rates. The following formula can be used to compute the non-dimension volume flow rate:

$$Q_m = \int_0^1 U dY \tag{29}$$

$$\begin{aligned}Q_m = &-\frac{A_0}{6}-\frac{A_1}{24}+\frac{D_3}{2}+D_2+M^2\left(-\frac{A_0}{120}-\frac{A_1}{720}+\frac{D_3}{24}+\frac{D_2}{6}\right)+\lambda\left[\frac{1}{120}+\frac{A_0}{120}+\frac{A_1}{720}\right.\\ &\left.(2-\varepsilon)\left(\frac{A_0^2}{120}+\frac{A_0A_1}{360}+\frac{A_1^2}{2520}\right)\right]-\frac{A_3}{24}-\frac{A_2}{6}+\frac{D_5}{2}+D_4\end{aligned} \tag{30}$$

And the heat transfer rate at both plates is calculated as:

$$Nu_0 = \frac{qb}{(T_1 - T_0)k} = \left.\frac{d\theta}{dy}\right|_{y=0} = A_1 + A_3 + A_5 \tag{31}$$

$$Nu_1 = \frac{qb}{(T_1 - T_0)k} = \left.\frac{d\theta}{dy}\right|_{y=1} = A_1 - \lambda\left[1 + A_0 + \frac{A_1}{2} + (2-\varepsilon)\left(A_0^2 + A_0A_1 + \frac{A_1^2}{3}\right)\right] + A_3 - (4\lambda - 2\varepsilon\lambda)\left[\frac{A_0}{6} + \frac{A_0^2}{6} + \frac{A_0A_1}{24}\right.$$
$$(2-\varepsilon)\left(\frac{A_0^3}{6} + \frac{A_0^2A_1}{12} + \frac{A_0A_1^2}{60}\right) + \frac{A_0A_3}{2} + A_0A_2 - \lambda\left\{\frac{A_1}{8} + \frac{A_0A_1}{8} + \frac{A_1^2}{60} + (2-\varepsilon)\left(\frac{A_0^2A_1}{8} + \frac{A_1^2A_0}{10} + \frac{A_1^3}{72}\right)\right\} + \frac{A_3A_1}{3} + \frac{A_0A_1}{2}\Big] + \lambda^2\left\{\frac{1}{6} + \frac{A_0}{6} + \frac{A_1}{24} + \right. \tag{32}$$
$$\left.(2-\varepsilon)\left(\frac{A_0^2}{6} + \frac{A_0A_1}{12} + \frac{A_1^2}{60}\right)\right\} + \lambda\left(\frac{A_3}{2} + A_2\right) + A_5$$

We obtained the sheer stress (τ) at the plates as follows

$$sk\ \inf\ riction(\tau_0) = \left.\frac{dU}{dy}\right|_{y=0} = D_3 + D_5 \tag{33}$$

$$sk\ \inf\ riction(\tau_1) = \left.\frac{dU}{dy}\right|_{y=1} = -A_0 - \frac{A_1}{2} + D_3 + M^2\Big($$
$$-\frac{A_0}{6} - \frac{A_1}{24} + \frac{D_3}{2} + D_2\Big) + \lambda\left\{\frac{1}{6} + \frac{A_0}{6} + \frac{A_1}{24} + (2-\varepsilon)\left(\frac{A_0^2}{6} + \frac{A_0A_1}{12} + \frac{A_1^2}{60}\right)\right\} - \frac{A_3}{2} + A_2 + D_5 \tag{34}$$

The appendix contains a list of all the constants utilized.

4. Discussion of the results

The effects of the chemical reaction parameter (λ), magnetic number (M), rarefaction parameter ($\beta_v Kn$), fluid-wall interaction parameter (In), and wall-ambient temperature difference ratio (ξ) are studied for a steady-state natural convection and heat flow problem. To demonstrate the influence of these relevant parameters, Figs. 2–10 and Tables 1 and 2 exhibits the fluctuation of energy, volume flow rate, momentum, and various physical characteristics of engineering significance such as the frictional force and the amount of heat transfer. The current calculation was performed between a reasonable interval of $0 \le \beta_v Kn \le 0.1$, and $0 \le$ In $\le$ 10 in the continuum and slip-flow region ($Kn \le 0.1$). The result of ($\beta_v Kn$) represents a degree of departure from the continuum regime, while (In) represents a feature of the fluid-wall interaction. According to Chen and Weng [6], the standard values for ($\beta_v Kn$) and (In) are 0.05 and 1.667, respectively, and M = 2 was used by Jha et al. [2]. Additionally, for this computation, the default values employed are $\lambda = 0.01$ and $\varepsilon = 0.01$ to elucidate the actions of various flow configurations.

Fig. 2(a–c) and 3(a - c) demonstrate the functions of λ and ξ based on the temperature and velocity distributions for each of the three cases of the wall-ambient temperature difference ratio; ($\xi = -1$: one wall is cooling and the other wall is heating; $\xi = 0$: one wall is not heating and the other wall is heating, $\xi = 1$: the case were both walls are heated). It is readily evident that when the value of (λ) grows, the temperature jump rises significantly. Similarly, it was established that as the value of (λ) increases, the flow movement accelerates. Also, as the velocity slip expands at the micro-channel wall, the fluid surface impact diminishes, leading to a surge in the speed of gas at

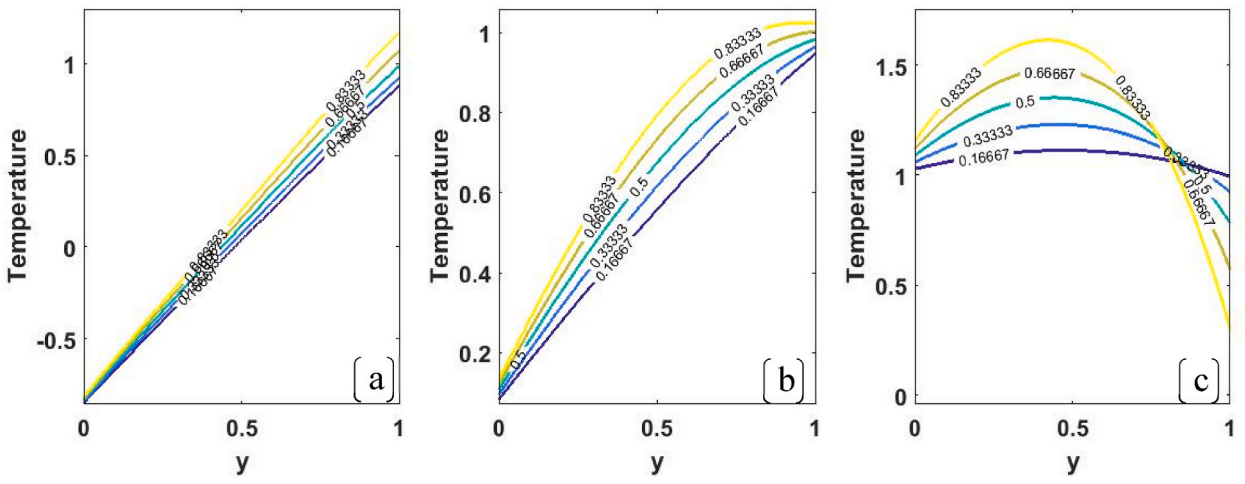

Fig. 2. Temperature distribution for λ at (a) $\xi = -1$, (b) $\xi = 0$ and (c) $\xi = 1$.

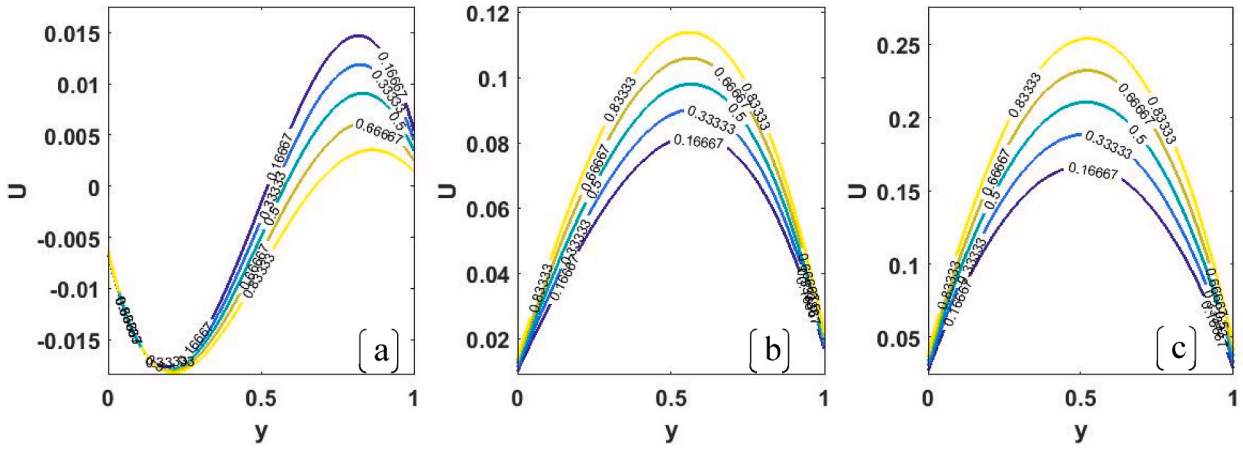

Fig. 3. Velocity distribution for λ at (a) $\xi = -1$, (b) $\xi = 0$ and (c) $\xi = 1$.

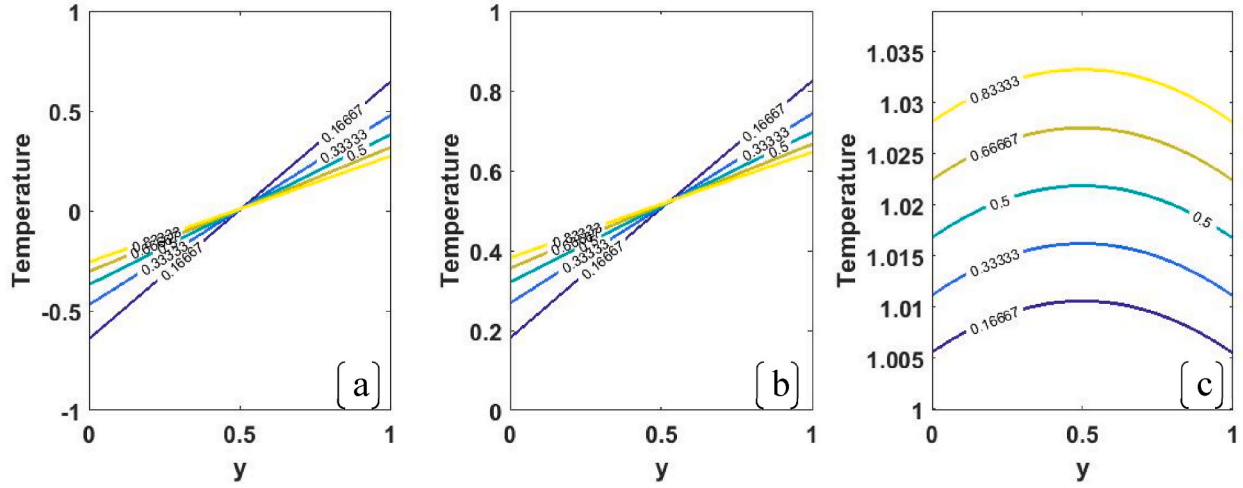

Fig. 4. $\beta_v Kn$ on the temperature profile at (a) $\xi = -1$, (b) $\xi = 0$ and (c) $\xi = 1$.

the boundary of the channel. This result corroborates those of Obalalu et al. [31] and Hamza [29].

Fig. 4(a–c) and 5(a - c) describe the variations of rarefaction parameters $(\beta_v Kn)$ on the temperature and velocity profiles respectively. These figures revealed that, as $(\beta_v Kn)$ levels are raised, the velocity slip at the surface is strengthened, which contributes to a decaying tendency at the walls. This effect yields a noticeable spike in the gas velocity near the wall. In addition, increasing $(\beta_v Kn)$ the parameter makes the temperature to jump significantly and lowers the rate of heat transfer from the wall to the fluid. These findings coincide with those obtained by Ojemeri and Hamza [32].

The fluctuations of (λ) on the volume flow is portrayed in Fig. 6(a–c). It is worthy of note that growing values of (λ) yield a noticeable enhancement in the volume flow rate as asserted by Ojemri and Hamza [32].

For different ascending values of (ξ), Fig. 7(a–c) and 8(a - c) demonstrate the variation of sheer stress versus $(\beta_v Kn)$ parameter for (λ) at both micro-channel plates. It is plain from the figures, uplifting the chemical reactant parameter empowers the skin friction at $y = 0$ whereas the reverse case happens at $y = 1$. The actions of $(\beta_v Kn)$ and (λ) on the heat transfer gradient are depicted in Fig. 9(a–c) and 10(a - c). It is worth mentioning that at $y = 0$, a drastic growth in the rate of heat transfer is recorded as $(\beta_v Kn)$ and (λ) factors are raised respectively, while at $y = 1$, the opposite effect is observed, as displayed in these figures.

5. Validation

To confirm the accuracy of our study, we compare the numerical results from Jha et al. [2] to the present investigation to verify its precision. Tables 1 and 2 demonstrate how the comparison for velocity and volume flow rate were in good agreement. The accuracy of the present solution, using three terms of the homotopy perturbation approach, confirms the fast convergence of the technique and proves that the homotopy perturbation technique is a suitable tool for solving nonlinear differential equation problems.

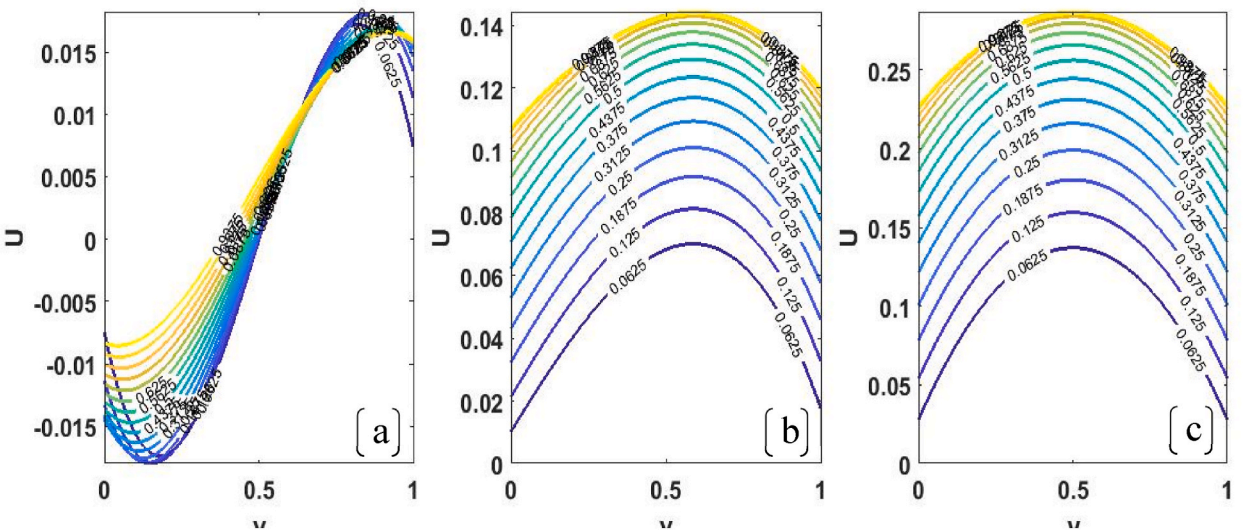

Fig. 5. $\beta_v Kn$ on the velocity profile at (a) $\xi = -1$, (b) $\xi = 0$ and (c) $\xi = 1$.

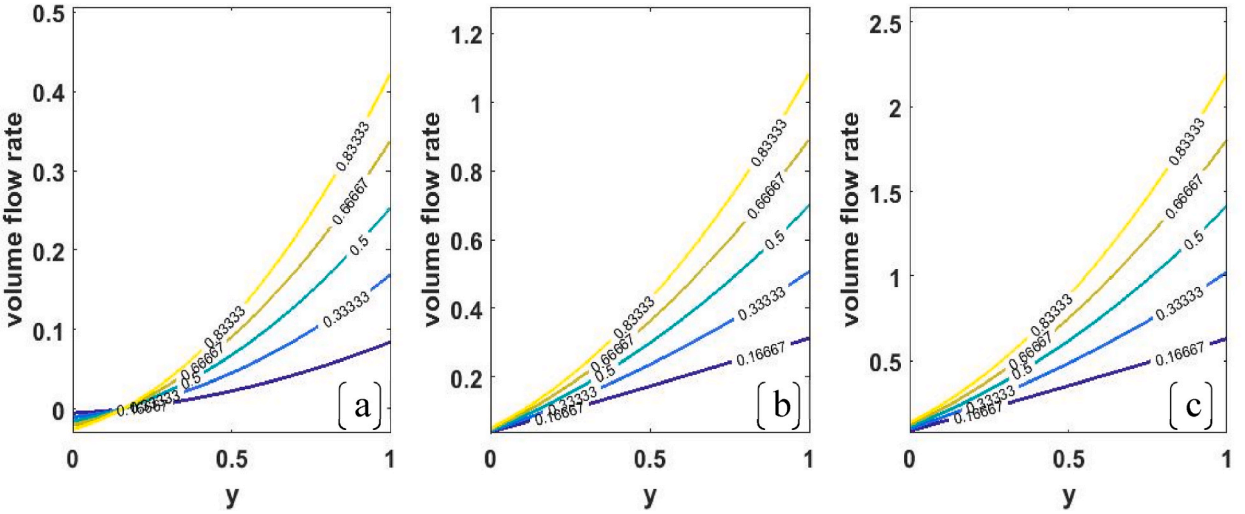

Fig. 6. Volume flow rate for λ at (a) $\xi = -1$, (b) $\xi = 0$ and (c) $\xi = 1$.

6. Conclusion

The analysis of steady-state free MHD flow of a chemically reactive, and electrically conducting fluid in a micro-channel was performed using the homotopy perturbation method. Analytical solutions have been derived for temperature, frictional force, velocity, heat transfer rate, and volume flow. The effects of controlling factors such as rarefaction parameters, chemically reacting parameters, magnetic number, wall ambient temperature difference ratio parameters, and fluid wall interaction parameters were estimated, and the results were detailed using mesh grid graphs. A summary of the noteworthy outcomes is highlighted below.

i It is revealed that an escalation in the fluid velocity and volume flow rate is noticed as the chemical reacting parameter, λ and rarefaction, $\beta_v Kn$ term increase.
ii Similarly, higher levels of reaction rate parameter, λ and rarefaction, $\beta_v Kn$ factor improve the temperature profile significantly.
iii As the reaction rate parameter, λ and rarefaction, $\beta_v Kn$ factor are uplifted, the skin friction impact becomes stronger at y = 0, whereas it diminishes at y = 1.
iv As the fluid is heated at y = 0, the rate of heat transfer increases dramatically with increasing values of rarefaction, $\beta_v Kn$ factor, and chemically reacting parameters, λ, whereas a contrast phenomenon occurs at y = 1.

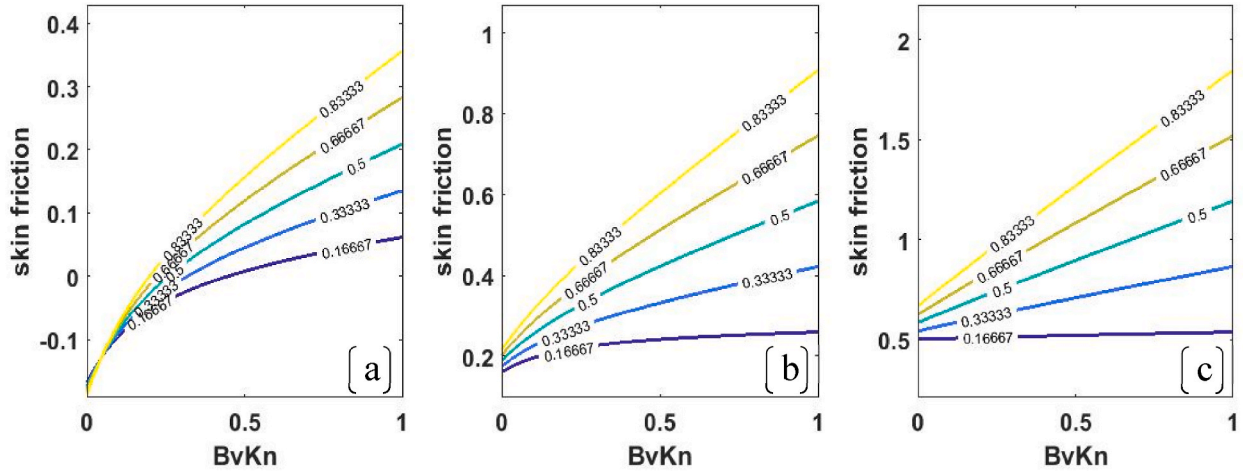

Fig. 7. Skin friction at y = 0 versus $\beta_v Kn$ for various values of λ at (a) $\xi = -1$, (b) $\xi = 0$ and (c) $\xi = 1$.

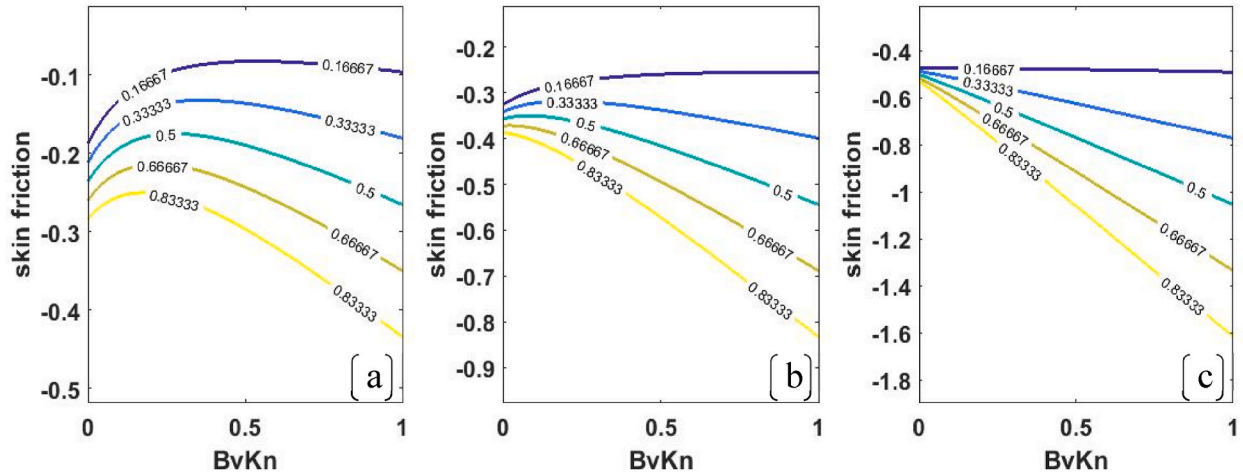

Fig. 8. Skin friction at y = 1 versus $\beta_v Kn$ for various values of λ at (a) $\xi = -1$, (b) $\xi = 0$ and (c) $\xi = 1$.

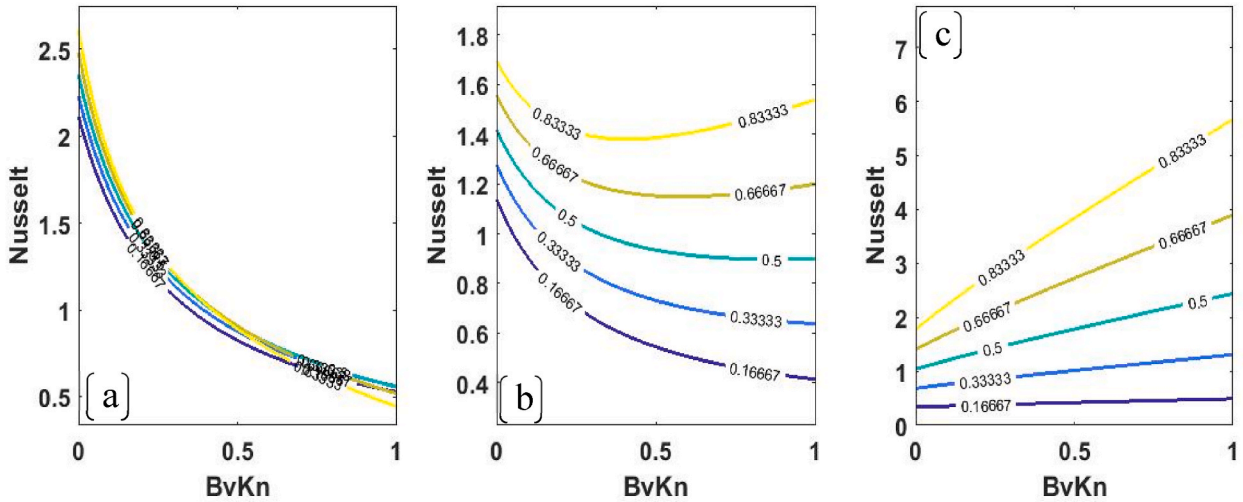

Fig. 9. Nusselt number at y = 0 versus $\beta_v Kn$ for various values of λ at (a) $\xi = -1$, (b) $\xi = 0$ and (c) $\xi = 1$.

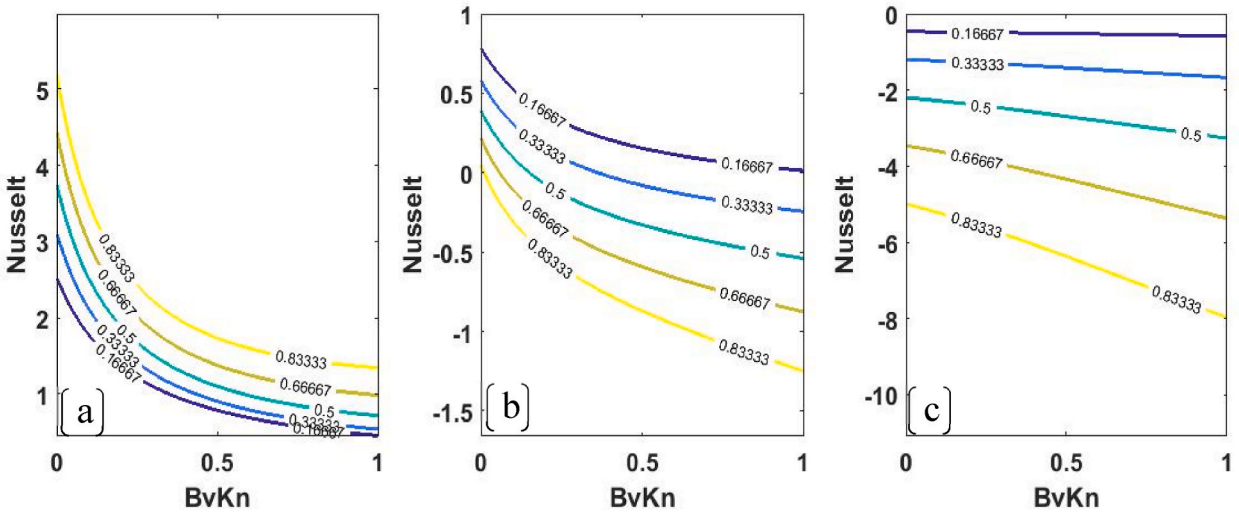

Fig. 10. Nusselt number at y = 1 versus $\beta_v Kn$ for various values of λ at (a) $\xi = -1$, (b) $\xi = 0$ and (c) $\xi = 1$.

Table 1
Numerical comparison of the current study on the velocity gradient with the work of Jha et al. [2], for $\xi = -1, 0, 1$ at $\beta_v Kn = 0.05$, In = 1.667, M = 1 as $\lambda \to 0$.

Y	Jha et al. [2] U(Y)			Present work U(Y)		
	$\xi = -1$	$\xi = 0$	$\xi = 1$	$\xi = -1$	$\xi = 0$	$\xi = 1$
0.1	0.0068	0.0156	0.0244	0.0068	0.0155	0.0243
0.2	0.0067	0.0153	0.0239	0.0066	0.0152	0.0239
0.3	0.0066	0.0150	0.0235	0.0065	0.0150	0.0234
0.4	0.0065	0.0148	0.0230	0.0064	0.0147	0.0230
0.5	0.0063	0.0145	0.0226	0.0063	0.0144	0.0225

Table 2
Numerical comparison of the current study on the velocity gradient with the work of Jha et al. [2], using volume flow rate for $\xi = 0$ *and* 1 at $\beta_v Kn = 0.0$, 0.05, and 0.1, In = 1.667, M = 1 as $\lambda \to 0$.

$\beta_v Kn$	Jha et al. [2] Q_m		Present work Q_m	
	$\xi = 0$	$\xi = 1$	$\xi = 0$	$\xi = 1$
0.0	0.0379	0.0758	0.0375	0.0751
0.05	0.0479	0.0958	0.0472	0.0953
0.1	0.0575	0.1150	0.0571	0.1143

Author contribution statement

Muhammed Murtala Hamza, Samaila Kenga-kwai Ahmad: Conceived and designed the experiments; Contributed reagents, materials, analysis tools or data.

Godwin Ojemeri: Analyzed and interpreted the data; Performed the experiments; Wrote the paper.

Data availability statement

Data will be made available on request.

Declaration of competing interest

The authors declare that they have no known competing financial interests or personal relationships that could have appeared to influence the work reported in this paper.

Appendix

$$A_0 = \xi + \frac{BnKnIn(1-\xi)}{1+2BnKnIn}, A_1 = \frac{(1-\xi)}{1+2BnKnIn}, A_2 = BnKnInA_3$$

$$A_3 = \frac{\lambda BnKnIn(c_4 - c_5 + c_6) + \lambda(c_1 - c_2 + c_3)}{1+2BnKnIn}, A_4 = BnKnInA_5,$$

$$-BnKnIn(-c_{20} + c_{21} - c_{22} - c_{23} + c_{24} - c_{25} + c_{26} - c_{27} + c_{28} - c_{29} + c_{30} + c_{31})$$

$$+\lambda(4\lambda - 2e\lambda)(c_8 - c_9 + c_{10}) + c_{11}(4\lambda - 2e\lambda)(c_{12} - c_{13} + c_{14}) + c_{15}(4\lambda - 2e\lambda)$$

$$A_3 = \frac{-\lambda^2(c_{16} - c_{17} + c_{18}) - c_{19}}{1+2BnKnIn}$$

$$D_2 = BnKnD_3, D_3 = \frac{BnKnA_0 + BnKn\frac{A_1}{2} + \frac{A_0}{2} + \frac{A_1}{6}}{(1+2BnKn)}$$

$$D_4 = BnKnD_5, D_5 = \frac{-BnKnc_{35} - \lambda BnKn(c_{36} - c_{37} + c_{38}) - BnKnc_{39} - c_{30} - c_{34} - \lambda(c_{31} + c_{32} + c_{34})}{(1+2BnKn)}$$

$$c_1 = \frac{1}{2} + \frac{A_0}{2} + \frac{A_1}{2}, c_2 = e\left(\frac{A_0^2}{2} + \frac{A_0A_1}{3} + \frac{A_1^2}{12}\right), c_3 = 2\left(\frac{A_0^2}{2} + \frac{A_0A_1}{3} + \frac{A_1^2}{12}\right)$$

$$c_4 = 1 + A_0 + \frac{A_1}{2}, c_5 = e\left(A_0^2 + A_0A_1 + \frac{A_1^2}{3}\right), c_6 = 2\left(A_0^2 + A_0A_1 + \frac{A_1^2}{3}\right),$$

$$c_8 = \frac{A_0}{24} + \frac{A_0^2}{24} + \frac{A_0A_1}{120}, c_9 = e\left(\frac{A_0^3}{24} + \frac{A_0^2A_1}{60} + \frac{A_0A_1^2}{360}\right), c_{10} = 2\left(\frac{A_0^3}{24} + \frac{A_0^2A_1}{60} + \frac{A_0A_1^2}{360}\right),$$

$$c_{11} = \frac{A_0A_3}{6} + \frac{A_0A_2}{2}, c_{12} = \left(\frac{A_1}{40} + \frac{A_0A_1}{40} + \frac{A_1^2}{180}\right), c_{13} = e\left(\frac{A_0^2A_1}{40} + \frac{A_1^2A_0}{60} + \frac{A_1^3}{504}\right),$$

$$c_{14} = 2\left(\frac{A_0^2A_1}{40} + \frac{A_1^2A_0}{60} + \frac{A_1^3}{504}\right), c_{15} = \frac{A_1A_3}{12} + \frac{A_1A_2}{6}, c_{16} = \frac{1}{24} + \frac{A_0}{24} + \frac{A_1}{120},$$

$$c_{17} = e\left(\frac{A_0^2}{24} + \frac{A_0A_1}{60} + \frac{A_1^2}{360}\right), c_{18} = 2\left(\frac{A_0^2}{24} + \frac{A_0A_1}{60} + \frac{A_1^2}{360}\right), c_{19} = \lambda\left(\frac{A_3}{6} + \frac{A_2}{2}\right),$$

$$c_{20} = \frac{A_0}{6} + \frac{A_0^2}{6} + \frac{A_0A_1}{24}, c_{21} = e\lambda(4\lambda - 2e\lambda)\left(\frac{A_0^3}{6} + \frac{A_0^2A_1}{12} + \frac{A_0A_1^2}{60}\right),$$

$$c_{22} = 2\lambda(4\lambda - 2e\lambda)\left(\frac{A_0^3}{6} + \frac{A_0^2A_1}{12} + \frac{A_0A_1^2}{60}\right), c_{23} = (4\lambda - 2e\lambda)\left(\frac{A_0A_3}{2} + A_0A_2\right),$$

$$c_{24} = \lambda\left(\frac{A_1}{8} + \frac{A_0A_1}{8} + \frac{A_1^2}{30}\right), c_{25} = e\lambda(4\lambda - 2e\lambda)\left(\frac{A_0^2A_1}{8} + \frac{A_1^2A_0}{15} + \frac{A_1^3}{72}\right),$$

$$c_{26} = 2\lambda(4\lambda - 2e\lambda)\left(\frac{A_0^2A_1}{8} + \frac{A_1^2A_0}{15} + \frac{A_1^3}{72}\right), c_{27} = (4\lambda - 2e\lambda)\left(\frac{A_1A_3}{3} + \frac{A_1A_2}{2}\right),$$

$$c_{28} = \lambda^2\left(\frac{1}{6} + \frac{A_0}{6} + \frac{A_1}{24}\right), c_{29} = e\lambda^2\left(\frac{A_0^2}{6} + \frac{A_1A_0}{12} + \frac{A_1^2}{60}\right), c_{29} = 2\lambda^2\left(\frac{A_0^2}{6} + \frac{A_1A_0}{12} + \frac{A_1^2}{60}\right),$$

$$c_{31} = \lambda\left(\frac{A_3}{2} + A_2\right), c_{32} = -\frac{A_0}{24} - \frac{A_1}{120} + \frac{D_3}{6} + \frac{D_2}{2}, c_{33} = \frac{1}{24} + \frac{A_0}{24} + \frac{A_1}{120},$$

$$c_{34} = e\left(\frac{A_0^2}{24} + \frac{A_0A_1}{60} + \frac{A_1^2}{360}\right), c_{35} = 2\left(\frac{A_0^2}{24} + \frac{A_0A_1}{60} + \frac{A_1^2}{360}\right), c_{36} = -\frac{A_3}{6} - \frac{A_2}{2},$$

$$c_{37} = M^2\left(-\frac{A_0}{6} - \frac{A_1}{24} + \frac{D_3}{2} + D_2\right), c_{38} = \frac{1}{6} + \frac{A_0}{6} + \frac{A_1}{24}\right), c_{39} = e\left(\frac{A_0^2}{6} + \frac{A_1A_0}{12} + \frac{A_1^2}{60}\right),$$

$$c_{40} = 2\left(\frac{A_0^2}{6} + \frac{A_1A_0}{12} + \frac{A_1^2}{60}\right), c_{41} = -\frac{A_3}{2} - A_2$$

Nomenclature

B_0	constant magnetic flux density
g	gravitational acceleration
b	channel width
CpCv	specific heats at constant pressure and constant volume respectively
$f_p f_v$	thermal and tangential momentum accommodation coefficients, respectively
In	fluid -wall interaction parameter
Kn	Knudsen number a/b
λ	chemical reactant parameter
Q	dimensionless volume flow rate
M	Hartmann number
Pr	Prandtl number
Nu	dimensionless heat transfer rate
e	activation energy
T	temperature of the fluid
T0	reference temperature
u	velocity component in x direction
U	dimensionless velocity

Greek letters

β	thermal expansion coefficient
$\beta_t \beta_v$	dimensionless variables
μ	dynamic viscosity
α	thermal diffusivity
γ_s	ratios of specific heats (CpCv)
ξ	wall-ambient temperature difference ratio
σ	electrical conductivity of the fluid
ρ	density
v	fluid kinematic viscosity

References

[1] M.A. Al-Nimr, A.F. Khadrawi, Thermal behavior of a stagnant gas confined in a horizontal microchannel as described by the dual-phase-lag heat conduction model, Int. J. Thermophy 25 (2) (2004) 1953–1964.

[2] B.K. Jha, B. Aina, A.T. Ajiya, MHD natural convection flow in a vertical parallel plate microchannel, Ain Shams Eng. J. 6 (2014) 289–295.

[3] B.K. Jha, P.B. Malgwi, Hall current and ion – slip effects on free convection flow in a vertical microchannel with induced magnetic field, Heat Tran. Asian Res. 48 (8) (2019) 1–19.

[4] B.K. Jha, B. Aina, Role of induced magnetic field on MHD natural convection flow in vertical microchannel formed by two electrically non-conducting infinite vertical parallel plates, Alex. Eng. J. 55 (2) (2016) 2087–2097.

[5] B.K. Jha, P.B. Malgwi, B. Aina, Hall Effects on MHD Natural Convection Flow in a Vertical Microchannel, Alexandria Eng. J, 2017, https://doi.org/10.1016/j.aej.2017.01.038.

[6] C.K. Chen, H.C. Weng, Natural convection in a vertical micro-channel, J. Heat Tran. 127 (2005) 1053–1056.

[7] B.K. Jha, B. Aina, Mathematical modelling and exact solution of steady fully developed mixed convection flow in a vertical micro-porous-annulus, J. Afrika Matem-atika 26 (2015) 1199–1213.

[8] B. Buonomo, O. Manca, Natural convection flow in a vertical micro-channel with heated at uniform heat flux, Int. J. Therm. Sci. 49 (2012) 1333–1344.

[9] H.C. Weng, C.K. Chen, Drag reduction and heat transfer enhancement over a heated wall of a vertical annular microchannel, Int. J. Heat Mass Tran. 52 (2009) 1075–1079.

[10] B.K. Jha, Babatunde Aina, S.B. Joseph, Natural convection flow in vertical micro-channel with suction/injection, J. Proc. Mech. Eng. 228 (3) (2014) 171–180.

[11] B.K. Jha, B. Aina, S. Isa, Fully developed MHD natural convection flow in a vertical annular microchannel: an exact solution, J. King Saud Univ. Sci. 27 (2015) 253–259.

[12] Y. Chu, S. Bilal, M.R. Hajizadeh, Hybrid ferrfluid along with MWCNT for augmentation of thermal behavior of fluid during natural convection in a cavity, Math. Methods Appl. Sci. (2020), https://doi.org/10.1002/mma.6937.

[13] T. Gul, K. Ullah, M. Bilal, W. Alghamdi, M.I. Asjad, T. Abdeljawad, Hybrid nanofluid flow within the conical gap between the cone and the surface of a rotating disk, Sci. Rep. 11 (2021) 11–18.

[14] T. Islam, N. Md Alam, M.I. Asjad, N. Parveen, Y. Chu, Heatline visualization of MHD natural convection heat transfer of nanofluid in a prismatic enclosure, Sci. Rep. 11 (2021), 10972.

[15] A. Saeed, T. Gul, Bioconvection casson nanofluid flow together with Darcy-Forchheimer due to a rotating disk with thermal radiation and Arrhenius activation energy, SN Appl. Sci. 3 (2021) 78.

[16] M. Ibrahim, T. Saeed, E.A. Algehyne, H. Alsulami, Y. Chu, Optimization and effect of wall conduct on natural convection in a cavity with constant temperature heat source using lattice Boltzmann method and neural network algorithm, Journal of thermal Analysis and Calometry 144 (2021) 2449–2463.

[17] A. Aziz, M. Shams, Entropy generation in MHD Maxwell nanofluid flow with variable thermal conductivity, thermal radiation, slip conditions, and heat source, AIP Adv. 10 (2020), 015038.

[18] P. Gurivireddy, M.C. Raju, B. Mamatha, S.K. Varma, Thermal diffusion effect on MHD heat and mass transfer flow past a semi-infinite moving vertical porous plate with generation and chemical reaction, Appl. Math. 7 (7) (2016) 638.

[19] K. Gangadhar, M. Aruna, M.A. Kumari, A.J. Chamkha, EMHD flow of radiative Second-Grade Nanofluid over a Riga plate due to convective heating: revised Buongiorno's Nanofluid model, Arabian J. Sci. Eng. 47 (2022) 8093–8103.
[20] K. Gangadhar, V.R. Kolipaula, M.V.S. Rao, S. Penki, A.J. Chamkha, Internal heat generation on bioconvection of an MHD nanofluid flow due to gyrotactic microorganisms, The European Physical Journal plus 135 (2020) 600.
[21] R. Muthuraj, S. Srinivas, Mixed convective heat and mass transfer in a vertical wavy channel with travelling thermal waves and porous medium, J. Comput. Math. Appl. 59 (2010) 3516–3528.
[22] D.A. Frank-Kamenetskii, Diffusion and Heat Transfer in Chemical Kinetics, Plenum Press, New York, 1969.
[23] O.D. Makinde, Thermal criticality in viscous reactive flows through channels with a sliding wall: an exploitation of the Hermite– Pade approximation method, J. Math. Comput. Model 47 (2008) 312–317.
[24] M.M. Hamza, G. Ojemeri, S. Abdulsalam, Mixed convection flow of viscous reactive fluids with thermal diffusion and radial magnetic field in a vertical porous annulus, Comput. math. mod 30 (3) (2019), https://doi.org/10.1007/510598-019-09451-0.
[25] G. Ojemeri, I.O. Onwubuya, S. Abdulsalam, Effects of Soret and Radial magnetic field of a free convection slip flow in a viscous reactive fluid towards a vertical porous cylinder, Cont. J. Applied Sci 14 (1) (2019) 25–45, https://doi.org/10.5281/zenodo.265200.
[26] K.S. Ahmad, B.K. Jha, Computational methods of transient/steady natural convection flow of reactive viscous fluid in vertical porous pipe, Asian J. Math. Comput. Res. 2 (2015) 74–92.
[27] B.K. Jha, A.K. Samaila, A.O. Ajibade, Transient free-convective flow of reactive viscous fluid in a vertical channel, Int. Commun. Heat Mass Tran. 38 (2011) 633–637.
[28] B.K. Jha, A.K. Samaila, A.O. Ajibade, Transient free-convective flow of reactive viscous fluid in a vertical tube, Int. Commun. Heat Mass Tran. 54 (2011) 2880–2888.
[29] M.M. Hamza, Free convection slip flow of an exothermic fluid in a convectively heated vertical channel, Ain Shams Eng. J. (2016), https://doi.org/10.1016/j.asej.2016.08.011.
[30] Z. Ayati, J. Biazar, On the convergence of homotopy perturbation method, J. Egyptian Math Soc. 23 (2015) 424–428.
[31] A.M. Obalalu, O.A. Ajala, A.T. Adeosun, A.O. Akindele, O.A. Oladapo, O.A. Olajide, Significance of variable electrical conductivity on non-Newtonian fluid flow between two vertical plates in the coexistence of Arrhenius energy and exothermic chemical reaction, Partial Diff. Eqn Appl Math 4 (2021) 1–9.
[32] G. Ojemeri, M.M. Hamza, Heat transfer analysis of Arrhenius-controlled free convective hydromagnetic flow with heat generation/absorption effect in a micro-channel, Alex. Eng. J. 61 (2022) 12797–12811.